Supplementary Material for *Thermal robustness of the quantum spin Hall phase in monolayer WTe_2*

Antimo Marrazzo[1]

[1] *Dipartimento di Fisica, Università di Trieste, Strada Costiera 11, I-34151 Trieste, Italy*[*]

(Dated: January 20, 2023)

Methods

First-principles simulations

Density-functional theory (DFT) calculations are performed with the Quantum ESPRESSO distribution [1] using the PBE functional [2]. Structural relaxations are performed without spin-orbit coupling (SOC) using the SSSP Efficiency library and cutoffs v1.1 [3, 4]. The equilibrium structure without the effect of zero-point motion is obtained with variable-cell structural optimization and the BFGS algorithm. Band structures with SOC are obtained through fully-relativistic norm-conserving PseudoDojo [5, 6] pseudopotentials with an 80 (320) Ry wavefunction (charge density) cutoff. The Coulomb cutoff [7, 8] is used to avoid spurious interactions between periodic replicas and thus simulate the correct boundary conditions for 2D systems.

Hybrid-functional calculations with SOC are performed using the Heyd-Scuseria-Ernzerhof (HSE) functional [9] and norm-conserving SG15 [5, 10] pseudopotentials, as implemented in Quantum ESPRESSO [1] with the acceleration provided by the Adaptively Compressed Exchange Operator [11]. HSE calculations for pristine WTe_2 are obtained with a 80 Ry cutoff for the wavefunction and the Fock operator, 320 Ry for the charge density, and with a k-grid of $14 \times 8 \times 1$ and a q-grid of $7 \times 4 \times 1$.

Band structures are interpolated using maximally-localized Wannier functions [12] as implemented in Wannier90 [13].

[*] antimo.marrazzo@units.it

Phonons and the quasi-harmonic approximation

Phonons are calculated on a 6×4×1 uniform q-point grid by using DFPT with pseudopotentials and cutoffs of the SSSP Efficiency library v1.1 [3, 4]. DFPT calculations are performed without SOC as the effect of the latter on the phonon frequencies is negligible; this is verified also by DFPT calculations at Γ with and without SOC using the PseudoDojo pseudopotentials: the frequency difference due to SOC is never larger than 1.4% on each mode individually. In the integration of the free energy, phonon frequencies are Fourier interpolated from the force constants to a 18×12×1 q-point grid. Phonons frequencies are calculated for 25 different lattice parameters that form a 5×5 uniform grid obtained by considering all the possible combinations of a and b strained by 0, ±1% and ±2% around the zero-temperature relaxed configuration. Then, the dependence of the phonon frequencies $\omega_{\mathbf{q},j}$ with respect to the a and b is fitted with a two-variable polynomial in order to calculate the vibrational energy F_{vib} at any desired lattice constant. Linear, quadratic and cubic polynomials are considered, the results are reported in Fig.1. The cubic and quadratic polynomials give very similar results until 1000 K, while the linear fitting starts to deviate significantly only starting at 500 K.

The electronic ground-state energy E is fitted with a two-variable quartic polynomial and added to F_{vib} obtain the Helmholtz free energy F. Finally, for each temperature the free energy is calculated on a dense grid in (a, b) and minimized it to obtain equilibrium lattice parameters $(a_{eq}(T), b_{eq}(T))$.

The equilibrium lattice constants represented by a triangle in Fig. 2 of the main text and in Supplementary Fig. 1 are obtained with variable-cell structural optimization and the BFGS algorithm.

Electron-phonon coupling and the special displacement method

The renormalization of the band structure due to the electron-phonon coupling is calculated by using the special displacement method [14] (SDM). The SDM is a non-perturbative approach where at each temperature the band structure is computed on a sufficiently large supercell constructed with atomic position which are suitably distorted according to the phonon displacement patterns calculated with DFPT. Thermal expansion is taken into ac-

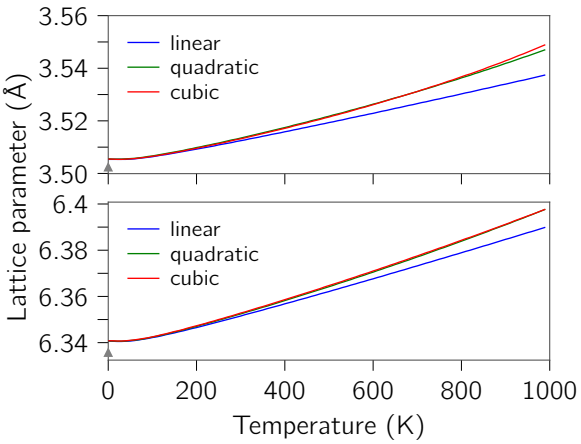

Supplementary Fig. 1. Equilibrium lattice parameters of monolayer WTe_2 from 0 to 1000 K calculated with the quasi-harmonic approximation. The three curves are obtained by considering a linear, quadratic and cubic polynomial for the fitting of the phonon frequencies with respect to the lattice constants. The triangles at 0 K represent the equilibrium lattice parameters obtained without considering the zero-point motion.

count by calculating the phonons with the equilibrium lattice constants obtained in the QHA. For improved accuracy, in the SDM we recalculate the phonons with a higher wavefunction and charge density cutoff, 80 Ry and 640 Ry respectively, using the SSSP pseudopotentials [3, 4]. At each temperature, a 6×3×1 supercell of 108 atoms is constructed starting from the real-space force constants, by using the ZG code [14] that is part of EPW [15]. Supercell PBE and HSE calculations are performed with SOC and Γ sampling. The wavefunction cutoff for supercell PBE calculations is equal to 80 Ry, while the corresponding cutoff for HSE calculations is set to 60 Ry and equal to the Fock cutoff. In the study of the effect of electron-phonon coupling on the band inversion, we include error bars to represent the uncertainty in the determination of the inversion strength at the Γ point. The bars account for the spectral broadening due to the unfolding procedure and include the intrinsic thermal broadening. Beyond the broadening, the spurious breaking of the band degeneracies is also included. The latter effect goes to zero in the infinite supercell limit, but it is always present in any tractable supercell. In the study of the indirect gap with HSE, we perform Wannier interpolation in the supercell BZ and represent with error bars

the spurious splitting of the band degeneracies due to the finite supercell.

---

[1] P. Giannozzi, O. Andreussi, T. Brumme, O. Bunau, M. Buongiorno Nardelli, M. Calandra, R. Car, C. Cavazzoni, D. Ceresoli, M. Cococcioni, N. Colonna, I. Carnimeo, A. Dal Corso, S. De Gironcoli, P. Delugas, R. A. Distasio, A. Ferretti, A. Floris, G. Fratesi, G. Fugallo, R. Gebauer, U. Gerstmann, F. Giustino, T. Gorni, J. Jia, M. Kawamura, H. Y. Ko, A. Kokalj, E. Kücükbenli, M. Lazzeri, M. Marsili, N. Marzari, F. Mauri, N. L. Nguyen, H. V. Nguyen, A. Otero-De-La-Roza, L. Paulatto, S. Poncé, D. Rocca, R. Sabatini, B. Santra, M. Schlipf, A. P. Seitsonen, A. Smogunov, I. Timrov, T. Thonhauser, P. Umari, N. Vast, X. Wu, and S. Baroni, Advanced capabilities for materials modelling with Quantum ESPRESSO, Journal of Physics Condensed Matter **29**, 465901 (2017).

[2] J. P. Perdew, K. Burke, and M. Ernzerhof, Generalized gradient approximation made simple, Phys. Rev. Lett. **77**, 3865 (1996).

[3] G. Prandini, A. Marrazzo, I. E. Castelli, N. Mounet, and N. Marzari, Precision and efficiency in solid-state pseudopotential calculations, npj Comput. Mater. **4**, 72 (2018).

[4] K. F. Garrity, J. W. Bennett, K. M. Rabe, and D. Vanderbilt, Pseudopotentials for high-throughput DFT calculations, Computational Materials Science **81**, 446 (2014).

[5] D. R. Hamann, Optimized norm-conserving Vanderbilt pseudopotentials, Phys. Rev. B **88**, 085117 (2013).

[6] M. J. van Setten, M. Giantomassi, E. Bousquet, M. J. Verstraete, D. R. Hamann, X. Gonze, and G. M. Rignanese, The PseudoDojo: Training and grading a 85 element optimized norm-conserving pseudopotential table, Comput. Phys. Commun. **226**, 39 (2018).

[7] C. A. Rozzi, D. Varsano, A. Marini, E. K. U. Gross, and A. Rubio, Exact Coulomb cutoff technique for supercell calculations, Phys. Rev. B **73**, 205119 (2006).

[8] T. Sohier, M. Calandra, and F. Mauri, Density functional perturbation theory for gated two-dimensional heterostructures: Theoretical developments and application to flexural phonons in graphene, Phys. Rev. B **96**, 075448 (2017).

[9] J. Heyd, G. E. Scuseria, and M. Ernzerhof, Hybrid functionals based on a screened coulomb potential, J. Chem. Phys. **118**, 8207 (2003).

[10] M. Schlipf and F. Gygi, Optimization algorithm for the generation of ONCV pseudopotentials, Computer Physics Communications **196**, 36 (2015).

[11] L. Lin, Adaptively compressed exchange operator, J. Chem. Theory Comput. **12**, 2242 (2016).

[12] N. Marzari, A. A. Mostofi, J. R. Yates, I. Souza, and D. Vanderbilt, Maximally localized Wannier functions: Theory and applications, Rev. Mod. Phys. **84**, 1419 (2012).

[13] G. Pizzi, V. Vitale, R. Arita, S. Blügel, F. Freimuth, G. Géranton, M. Gibertini, D. Gresch, C. Johnson, T. Koretsune, J. Ibañez-Azpiroz, H. Lee, J.-M. Lihm, D. Marchand, A. Marrazzo, Y. Mokrousov, J. I. Mustafa, Y. Nohara, Y. Nomura, L. Paulatto, S. Poncé, T. Ponweiser, J. Qiao, F. Thöle, S. S. Tsirkin, M. Wierzbowska, N. Marzari, D. Vanderbilt, I. Souza, A. A. Mostofi, and J. R. Yates, Wannier90 as a community code: new features and applications, J. Phys. Condens. Matter **32**, 165902 (2020).

[14] M. Zacharias and F. Giustino, Theory of the special displacement method for electronic structure calculations at finite temperature, Phys. Rev. Research **2**, 013357 (2020).

[15] S. Poncé, E. Margine, C. Verdi, and F. Giustino, EPW: Electron–phonon coupling, transport and superconducting properties using maximally localized Wannier functions, Computer Physics Communications **209**, 116 (2016).